Electronic phase diagram of valence-controlled cyanide: $Na_{0.84-\delta}Co[Fe(CN)_6]_{0.71}\cdot 3.8H_2O$ $(0 \leq \delta \leq 0.61)$

F. Nakada, H. Kamioka, and Y. Moritomo*
Department of Physics, University of Tsukuba, Tsukuba 305-8571, Japan

J. E. Kim
JASRI/SPring-8, 1-1-1 Kouto, Sayo-cho, Sayo-gun, Hyogo 679-5198, Japan

M. Takata
RIKEN SPring-8 Center, 1-1-1 Kouto, Sayo-cho, Sayo-gun, Hyogo 679-5148, Japan
and Department of Advanced Materials Science, The University of Tokyo, Kashiwa 277-8561, Japan
(Received 21 March 2008; revised manuscript received 29 May 2008; published 23 June 2008)

Electronic phase diagram has been derived for the Prussian-Blue-type cyano-bridged transition-metal compound, $Na_{0.84-\delta}Co[Fe(CN)_6]_{0.71}\cdot 3.8H_2O$ $(0.0 \leq \delta \leq 0.61)$, as a function of the hole concentration δ of the d-electron system. The mother compound ($\delta=0$) takes the Co^{2+} ($t_{2g}^5 e_g^2$:$S=3/2$) and Fe^{2+} (t_{2g}^6:$S=0$) configuration and is paramagnetic down to zero temperature. At room temperature, the holes are selectively introduced on the Fe site. A slight hole doping ($\delta=0.13$) causes the charge-transfer (CT) transition, that is, cooperative electron transfer from the Co^{2+} site to the Fe^{3+} site, with a decrease in temperature below $T_{CT} \approx 250$ K. With a further increase in δ, T_{CT} slightly decreases from ≈ 230 K at $\delta=0.24$ to ~ 210 K at $\delta=0.61$. Accordingly, the nature of the transition changes from the second-order type to the first-order type. In all the concentration ranges, the high-temperature (HT) phase is metastable even at low temperature. In this metastable phase, the Fe^{3+} (t_{2g}^5:$S=1/2$) species mediate the ferromagnetic exchange coupling between the adjacent Co^{2+} spins. The ferromagnetic transition appears at $\delta=0.39$, and the transition temperature T_C increase from 7 K at $\delta=0.39$ to 13 K at $\delta=0.61$. Based on these experimental data, we will discuss the significant roles of the coupling between the charge, spin, and lattice degrees of freedom in the transition-metal cyanides.

DOI: 10.1103/PhysRevB.77.224436 PACS number(s): 81.30.Dz, 78.66.Nk, 74.62.Bf, 81.05.Rm

I. INTRODUCTION

The phase diagram as a function of doping level (x) frequently contributes to the deeper comprehension of the electron systems and to the material design for realization of the unconventional physical properties as well as the giant response to the external stimuli. For example, in doped manganite, e.g., $Nd_{1-x}Sr_xMnO_3$, the charge degree of freedom couples with the spin and orbital degrees of freedom and causes a variety of spin-charge-orbital ordered states.[1] In the lightly doped region ($x \leq 0.48$), $Nd_{1-x}Sr_xMnO_3$ is ferromagnetic and metallic due to the double-exchange mechanism.[2] In the vicinity of the half-doping ($x \approx \frac{1}{2}$), a charge-ordered phase appears below $T_{CO}=150$ K (Ref. 3) with $d_{3x^2-r^2}/d_{3y^2-r^2}$ as the orbital alternation. With further doping, the $d_{x^2-y^2}$ ($d_{3z^2-r^2}$) orbital ordered phase appears at $x=0.52$ ($x=0.65$). Such a successive phase change is well explained by the double-exchange model with explicitly including the orbital degree of freedom.[4–6] The phase diagram of doped manganite stimulates the material scientists and triggers many findings.[1]

The hole-doping procedure is also possible in the Prussian-Blue-type cyano-bridged transition-metal compound, $A_xM[M'(CN)_6]_y\cdot zH_2O$ (A, M, and M' are alkaline metal, transition metal, and transition metal, respectively). Crystallographically, the compound belongs to the face-centered cubic ($Fm\bar{3}m$; $Z=4$), in which Co and Fe ions form a rocksalt-type (NaCl-type) network with sharing cyano (CN^-) moieties—CN-M-NC-M'-CN-M-.[7] The nanospaces formed by the network accommodate the alkaline metal ions (A^+) and a part of water molecules (zerolite water). The residual water molecules (ligand water) occupy the vacancy of the $[M'(CN)_6]$ site and coordinate with the M site. We can remove A from the nanospaces by an electrochemical method[8] and introduce the holes on the d-electron system.[9]

Among the cyano-bridged transition-metal cyanides, the Co-Fe compound is most extensively investigated because they show a charge-transfer (CT) transition from the high-temperature phase [$Co^{2+}(t_{2g}^5 e_g^2)$-$Fe^{3+}(t_{2g}^5)$: HT phase] to the low-temperature phase [$Co^{3+}(t_{2g}^6)$-$Fe^{2+}(t_{2g}^6)$: LT phase].[10] This CT transition accompanies a significant increase in the lattice constant a from ≈ 9.9 Å in the LT phase to ≈ 10.3 Å in the HT phase. The compound further shows the photoinduced magnetization[11,12] as well as the photoinduced structural change.[13] At low temperatures (≤ 150 K), the photoexcitation induces the phase transition from the LT phase to the magnetic HT phase.[10,13] Sato *et al.*[11] reported the enhancement of the magnetization in $K_{0.14}Co[Fe(CN)_6]_{0.71}\cdot 4.93H_2O$ by irradiation of a red light (660 nm) at 5 K and suppression of the magnetization by irradiation of a blue light (450 nm) at 5 K.

So far, Shimamoto *et al.*[10] investigated the chemical composition effects on the CT transition in $Na_xCo[Fe(CN)_6]_y\cdot zH_2O$ powders, which were synthesized by a solution reaction procedure with controlling the NaCl concentration and temperature. They find a systematic increase in the critical temperature (T_{CT}) for the CT transition with an increase in the NaCl concentration. The authors as-

cribed the increase in T_{CT} to the decrease in the vacancy concentration $(1-y)$ of $[Fe(CN)_6]$ because it strengthens the ligand field at the Co site to stabilize the LT phase. The solution reaction procedure, however, alters not only $1-y$ but also the Na concentration (x) and water content (z). In addition, the obtained powders are not suitable for the optical measurement, especially for the time-resolved spectroscopy,[14–16] due to the intense light scattering. These situations may discourage the quantitative argument on the experimental data.

In this paper, we have prepared a series of valence-controlled Co-Fe cyanide films, $Na_{0.84-\delta}Co[Fe(CN)_6]_{0.71}\cdot 3.8H_2O$ $(0.0\leq\delta\leq 0.61)$, by an electrochemical method without changing vacancy concentration or the water content. Here, note that the parameter δ represents the concentration of the trivalent transition metal per a Co site: the chemical formula, $Na_{0.84-\delta}Co[Fe(CN)_6]_{0.71}\cdot 3.8H_2O$, can be expressed as $Na^{I}_{0.84-\delta}Co^{II}[Fe^{II}(CN)_6]_{0.71-\delta}[Fe^{III}(CN)_6]_{\delta}\cdot 3.8H_2O$ in the HT phase. In an analogy of the perovskite oxide system, we will call δ as "hole" concentration of the *d*-electron system.[9] We have investigated the magnetic behavior of the films and derived the electronic phase diagram as a function of δ. Based on these experimental data, we will discuss the significant roles of the coupling between the charge, spin, and lattice degrees of freedom. We further systematically investigated the absorption spectra in the infrared and visible region. Based on the systematic change of the visible absorption spectra, we have decomposed the spectra into four optical transitions.

II. EXPERIMENT

A. Sample preparation and characterization

Films of the $Na_xCo[Fe(CN)_6]_y\cdot zH_2O$ were electrochemically synthesized on the indium tin oxide (ITO) transparent electrodes (sheet resistance was 100 Ω) under potentiostatic condition at 0.5 V versus a standard Ag/AgCl electrode in an aqueous solution containing 0.5 mmol/l $K_3[Fe^{III}(CN)_6]$, 1.25 mmol/l $Co^{II}(NO_3)_2$, and 1 mol/l $Na(NO_3)$. We added sawtoothed-type modulation (± 0.35 V and 71 Hz) to the applied potential. Before the film growth, the surface of the ITO electrode was purified by the electrolysis of water for several minutes. The obtained films were of transparent green. The elemental analysis by the inductively coupled plasma (ICP) method and CNH organic elementary analyzer (Perkin-Elmer 2400 CHN elemental analyzer) yields $Na_{0.84}Co[Fe(CN)_6]_{0.71}\cdot 3.8H_2O$. The film thickness was about 1000 nm, which was determined by the cross-sectional image of the scanning electron microscope (SEM). The x-ray diffraction pattern revealed that the compound is face-centered cubic with lattice constant $a=10.251$ Å.

The hole concentration δ of the film was controlled by the oxidization process of the film at 0.5–0.7 V versus a standard Ag/AgCl electrode in 1 mol/l $Na(NO_3)$ aqueous solution. The as-grown films that were synthesized with the sawtoothed-type potential modulation are strongly $\langle 111\rangle$ oriented, as revealed by the intense (111) Bragg reflection in the x-ray diffraction pattern. The orientation remains even after the oxidization process. We have investigated the film surface by SEM and found that the cubic crystals, whose size is ~ 100 nm, point their corners upward.

B. Structural and magnetic measurements

In order to investigate the structural properties of the hole-doped Co-Fe cyanide films, x-ray powder-diffraction patterns were measured at the synchrotron-radiation facility, SPring-8. First, the film was carefully removed from the ITO glass with a microspatula, and then the fine powders were filled into 0.5 mmϕ glass capillary. The capillary was sealed up and was put on a Debye-Scherrer camera at the BL02B2 beamline[17] of SPring-8. The wavelength of the x-ray was 0.801 65 Å, which was calibrated by the lattice constant of standard CeO_2 powders. The sample temperature was controlled by the cooled nitrogen gas. The exposure time was 5 min. The lattice parameters were refined by the Rietveld method with the face-centered-cubic $(Fm\bar{3}m; Z=4)$ model.

The magnetic properties of the hole-doped films were investigated with superconducting quantum interference device (SQUID) magnetometer (Quantum Design MPMS). In order to reduce the background magnetic susceptibility, the film was carefully removed from the ITO glass with a microspatula, and then the fine powders were filled into 0.5 mmϕ glass capillary. The background signal from the glass capillary is order of 10^{-6} emu, which is two order smaller than the signal from the sample powders. The typical sample mass was ~ 100 μg, which was estimated from the film thickness and the removed area with assuming the ideal density. We are careful enough to seal the glass capillary to keep the circumstance even in the SQUID magnetometer.

C. Optical measurement

The absorption spectra in the infrared region were measured with the use of an infrared microscope system (JASCO ITR-3000) equipped with a Fourier-transform-type infrared spectrometer. The transmitted light was focused on a cooled HgCdTe infrared detector. We posted a scotch tape on the film surface to reduce the interference effect. The absorption spectra in the visible to violet were measured with a conventional monochrometer system with a halogen lamp. The transmitted light was focused on a Si photodiode, and the lock-in detection was adopted to enhance the S/N ratio.

III. RESULTS

A. Valence control by an electrochemical method

We plotted in Fig. 1 the chemical composition of $Na_xCo[Fe(CN)_6]_y\cdot zH_2O$, that is, x, y, and z, as a function of the total charge q used in the oxidization process. We emphasize that that $y(=0.84)$ and $z(=3.8)$ are constant under the oxidation process. The Na concentration (x) decreases in proportion to q: $x=0.84-0.86q$. So, we used the empirical relation between q and x to estimate $\delta(=0.84-x)$. Here, note that δ represents the concentration of the trivalent transition metal per a Co site: the chemical formula, $Na_{0.84-\delta}Co[Fe(CN)_6]_{0.71}\cdot 3.8H_2O$, can be expressed as

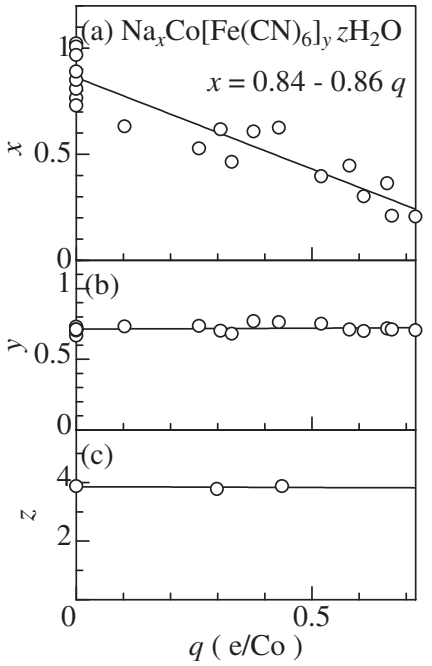

FIG. 1. Chemical composition of $Na_xCo[Fe(CN)_6]_y \cdot zH_2O$ films against the total charge q used in the oxidization process: (a) x, (b) y, and (c) z. The chemical composition was determined by the elemental analysis by the ICP method and the CNH organic elementary analyzer.

$Na^{I}_{0.84-\delta}Co^{II}[Fe^{II}(CN)_6]_{0.71-\delta}[Fe^{III}(CN)_6]_{\delta} \cdot 3.8H_2O$ in the HT phase. The x-ray diffraction pattern revealed that the hole-doped compounds are also face-centered cubic but a at 300 K slightly increases with δ: $a=10.270$ Å at $\delta=0.13$, $a=10.333$ Å at $\delta=0.39$, and $a=10.339$ Å at $\delta=0.61$.

Figure 2 shows the infrared-absorption spectra of the films at 300 K: (a) $\delta=0.00$, (b) $\delta=0.39$, and (c) $\delta=0.61$. In the as-grown film [(a) $\delta=0.00$], an intense absorption band is observed at 2080 cm^{-1}, which is ascribed to the stretching vibration mode of the CN moiety in the $[Fe^{II}(CN)_6]$ complex.[18] The intensity of the 2080 cm^{-1} band decreases with the increase in δ. Accordingly, a new absorption band appears at 2160 cm^{-1}, which is ascribed to the CN stretching mode of the $[Fe^{III}(CN)_6]$ complex.[18] In Fig. 3, we plotted the oscillator strength f for both the absorption bands against δ. The magnitude of f for the $[Fe^{II}(CN)_6]$ band linearly decreases with δ, while that for the $[Fe^{III}(CN)_6]$ band linearly increases. This clearly indicates that the holes are introduced on the Fe site at 300 K. It is interesting that the absolute magnitude of $f(=1.1\times10^{-3}/\mathrm{CN})$ for the $[Fe^{II}(CN)_6]$ band is much larger than that $(f=0.4\times10^{-3}/\mathrm{CN})$ for the $[Fe^{III}(CN)_6]$ band. This may reflect the different bonding electron distribution between $[Fe^{II}(CN)_6]$ and $[Fe^{III}(CN)_6]$, which is recently revealed by the maximum entropy method charge-density analysis.[19]

B. Electronic phase diagram

First, let us investigate the temperature dependence of the magnetic susceptibility χ on thin films of $Na_{0.84-\delta}Co[Fe(CN)_6]_{0.71} \cdot 3.8H_2O$. In Fig. 4, we show proto-

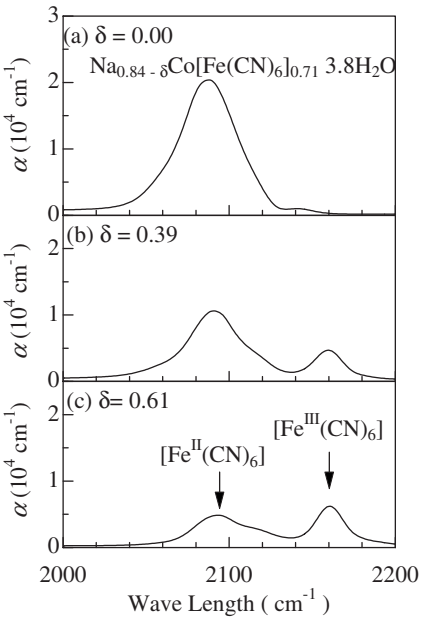

FIG. 2. Infrared absorption spectra of thin films of $Na_{0.84-\delta}Co[Fe(CN)_6]_{0.71} \cdot 3.8H_2O$ measured at 300 K: (a) $\delta=0.00$, (b) $\delta=0.39$, and (c) $\delta=0.61$. The higher- and lower-lying bands are ascribed to the CN stretching vibration of $[Fe^{II}(CN)_6]$ and $[Fe^{III}(CN)_6]$, respectively.

typical examples of χT against temperature T: (a) $\delta=0.00$, (b) $\delta=0.24$, and (c) $\delta=0.61$. The black curves were obtained in the cooling run under a magnetic field of 5000 G, while the gray curves were obtained in the warming run after the quench procedure at 5 K. In the as-grown film [(a) $\delta=0.00$], the $\chi T-T$ curve shows the Curie-type behavior (the black and red curves are completely overlapped). The estimated effective moment $\mu_{\mathrm{eff}}(=4.03\ \mu_B/\mathrm{Co})$ is close to the ideal value $(=3.87\ \mu_B/\mathrm{Co})$ for the high-spin Co^{2+} ions.

In the fully hole-doped sample [(c) $\delta=0.61$], several transitions are observed. Here, we emphasize that the chemical

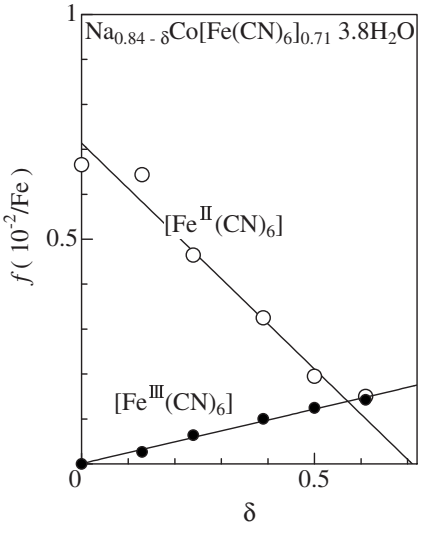

FIG. 3. Oscillator strength f of the CN stretching vibration of $[Fe^{II}(CN)_6]$ and $[Fe^{III}(CN)_6]$ at 300 K. The straight lines are the least-squares-fitted results.

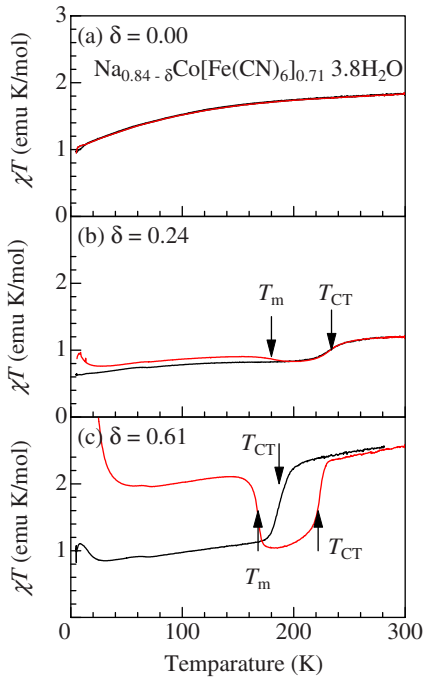

FIG. 4. (Color online) Temperature dependence of χT (where χ and T are susceptibility and temperature) of thin films of $Na_{0.84-\delta}Co[Fe(CN)_6]_{0.71}\cdot 3.8H_2O$: (a) δ=0.00, (b) δ=0.24, and (c) δ=0.61. The black curves were obtained in the cooling run under a magnetic field of 5000 G, while the gray curves were obtained in the warming run after the quench procedure at 5 K. T_{CT} and T_m represent the critical temperature of the CT transition and the melting temperature of the metastable phase.

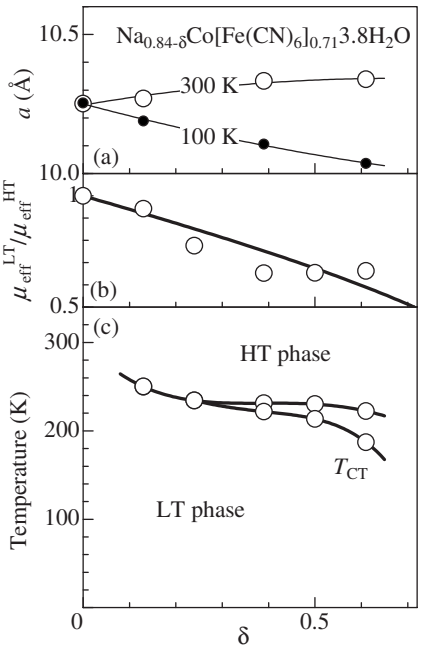

FIG. 5. (a) Lattice constant a at 300 K ($\geq T_{CT}$) and at 100 K ($\leq T_{CT}$) of thin films of $Na_{0.84-\delta}Co[Fe(CN)_6]_{0.71}\cdot 3.8H_2O$ against δ. (b) $\mu_{eff}^{LT}/\mu_{eff}^{HT}$ against δ, where μ_{eff}^{LT} (μ_{eff}^{HT}) is the effective moment in the LT (HT) phase. (c) Electronic phase diagram of thin films of $Na_{0.84-\delta}Co[Fe(CN)_6]_{0.71}\cdot 3.8H_2O$ against δ. The curves in (a) and (c) are merely the guide to the eyes. The curve in (b) is the calculation (see text).

composition at δ=0.61 ($Na_{0.23}Co[Fe(CN)_6]_{0.71}\cdot 3.8H_2O$) is close to that obtained by the solution reaction procedure (for example, compound 2 of Ref. 10: $Na_{0.27}Co[Fe(CN)_6]_{0.73}\cdot 3.5H_2O$). Actually, the $\chi T-T$ curve at δ=0.61 resembles that of $Na_{0.27}Co[Fe(CN)_6]_{0.73}\cdot 3.5H_2O$ powders.[10] With a decrease in temperature from 300 K [see the black curve of Fig. 4(c)], the χT shows steep reduction at 187 K. The reduction corresponds to the CT transition from the HT phase, $Co^{2+}(t_{2g}^5e_g^2)$-$Fe^{3+}(t_{2g}^5)$, to the LT phase, $Co^{3+}(t_{2g}^6)$-$Fe^{2+}(t_{2g}^6)$. One may notice that χT is fairly enhanced below T_m=160 K [see the red curve of Fig. 4(c)], reflecting the thermal quenching of the HT phase. Actually, the magnitude of μ_{eff} below T_m is nearly the same that above T_{CT}. The temperature T_m corresponds to the melting temperature of the metastable phase into the LT phase.[20] Here we note that T_m for the thermally quenched metastable phase is nearly the same as that for the photoinduced metastable phase in $Na_{0.42}Co[Fe(CN)_6]_{0.78}\cdot 4.64H_2O$ powders,[13] With a further increase in temperature, the CT transition from the LT phase to the HT phase takes place at T_{CT}=222 K. The corresponding anomalies due to the CT transition and the melting temperature are observed in the $\chi T-T$ curve at δ=0.24 [Fig. 4(b)]. The thermal hysteresis of the CT transition, however, almost disappears.

Thus obtained T_{CT} is plotted in Fig. 5(c) against δ. A slight hole doping (δ=0.13) causes the CT transition at $T_{CT}\approx$250 K. With a further increase in δ, T_{CT} slightly decreases from ≈230 K at δ=0.24 to ~210 K at δ=0.61. The weak correlation between T_{CT} and δ supports the idea that T_{CT} is mainly governed by the magnitude of the ligand field around the Co site.[10,21] Nevertheless, the nature of the transition changes from the second-order type without thermal hysteresis to the first-order type with significant hysteresis.

In Fig. 5(a), we plotted the lattice constant a at 300 K ($\geq T_{CT}$) and at 100 K ($\leq T_{CT}$), which were determined from the synchrotron-radiation x-ray powder-diffraction patterns. The conventional thermal contraction of a is negligible, as seen in the nondoped compound (δ=0.00). The magnitude of the lattice-constant change (Δa) at the CT transition seems to correlate with the nature of the transition; the larger Δa becomes, the larger the thermal hysteresis becomes. The slight reduction in T_{CT} with δ may be ascribed to the increase in a at 300 K because it weakens the ligand field around the Co site to stabilize the HT phase.

Here, let us consider the ratio of the charge-transferred Co site at the CT transition. If the charge transfer takes place between the Fe^{3+}-Co^{2+} pairs, the spin species of the system changes from Co^{2+} (S=3/2: density is 1) and Fe^{3+} (S=1/2:δ) to Co^{2+} (S=3/2:1−δ). Then, the magnitude of μ_{eff} decreases below T_{CT}, and the ratio $\mu_{eff}^{LT}/\mu_{eff}^{HT}$ is expressed as

$$\mu_{eff}^{LT}/\mu_{eff}^{HT} = \sqrt{\frac{15(1-\delta)}{15+3\delta}}, \quad (1)$$

where μ_{eff}^{LT} (μ_{eff}^{HT}) is the effective moment in the LT (HT) phase. In Fig. 5(b), we plotted experimentally obtained $\mu_{eff}^{LT}/\mu_{eff}^{HT}$ together with the above calculation. The calcula-

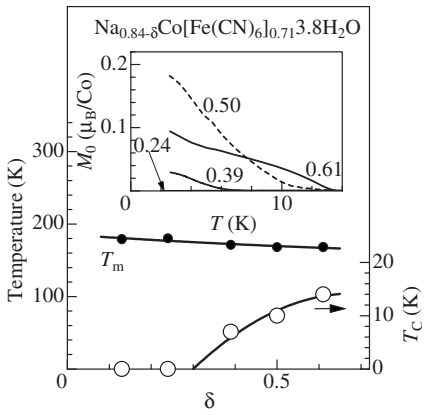

FIG. 6. The Curie temperature T_C (open circles) and the melting temperature T_m (filled circles) of the metastable phase of thin films of $Na_{0.84-\delta}Co[Fe(CN)_6]_{0.71}\cdot 3.8H_2O$ against δ. The inset shows temperature variation of the spontaneous magnetization M_0. M_0 was measured in the warming run in the zero field after the sample was cooled down to 2 K in the field of 5000 G.

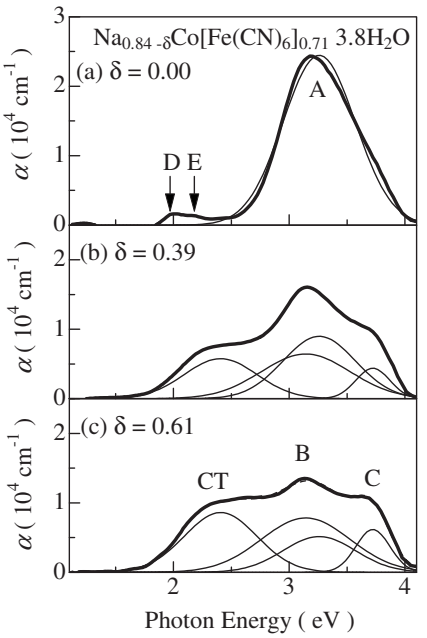

FIG. 7. Absorption spectra of thin films of $Na_{0.84-\delta}Co[Fe(CN)_6]_{0.71}\cdot 3.8H_2O$ measured at 300 K: (a) δ=0.00, (b) δ=0.39, and (c) δ=0.61. The thin curves represent the least-squares-fitting with the four Gauss-type absorption bands (the A, B, C, and CT bands). D and E bands can be ascribed to the intra-atomic $d-d$ transition of Co^{2+} (see text).

tion well reproduces the experimental data without any fitting parameters [see the curve in Fig. 5(b)]. This indicates that the ratio of the charge-transferred Co site at the CT transition is δ.

C. Magnetic phase diagram of the quenched phase

Now, let us proceed to the magnetic properties of the quenched HT phase. In this phase, the spin species are Co^{2+} (S=3/2: density is 1) and Fe^{3+} (S=1/2: δ). Then, the ferromagnetic coupling between the neighboring Co spins can be mediated by the antiferromagnetic superexchange coupling between the Co^{2+} and Fe^{3+}. In the inset of Fig. 6, we show temperature variation of the spontaneous magnetization M_0. In this measurement, the sample was cooled down to 2 K in the field of 5000 G. Then, M_0 was measured in the warming run in the zero field. Above δ=0.39, we observed finite M_0 value. The Curie temperature T_C increases with δ: T_C=7 K and δ=0.39, T_C=10 K at δ=0.50 and T_C=13 K at δ=0.61.

Thus obtained T_C (open circle) is plotted in Fig. 6 together with the melting temperature T_m (filled circle). With the increase in δ beyond ~0.3, T_C suddenly appears and then gradually increases. Such a behavior of T_C can be explained by the percolation theory. The introduced Fe^{3+} site mediated the ferromagnetic couplings among the surrounding six Co spins, causing a small ferromagnetic cluster of the Co site. The size of the ferromagnetic cluster increases with δ. The percolation theory tells us that the cluster size becomes infinite if δ exceeds a critical value p_c [=0.195 (Ref. 22)] for the face-centered-cubic lattice.

D. Electronic structure

Figure 7 shows the visible absorption spectra of the films at 300 K: (a) δ=0.00, (b) δ=0.39, and (c) δ=0.61. In the as-grown film [(a) δ=0.00], an intense absorption band is observed at 3.3 eV (A band) together with the weak absorptions around 2 eV (D and E bands). The D and E bands can be ascribed to the intra-atomic $d-d$ transition of Co^{2+}. Such a $d-d$ transition is dipole-forbidden within a center-symmetric (O_h) ligand field, that is, $Co[Fe(CN)_6]_6$. In an actual system, however, parts of the $[Fe(CN)_6]$ site are replaced by the ligand water. Then, the resultant asymmetric ligand field allows the $d-d$ transition via the strong hybridization between the Coe_g orbital and the CNσ^* orbital.[23] Actually, Ohkoshi *et al.*[24] reported a similar 2.0 eV band in $(Co^{II}_{0.41}Mn^{II}_{0.59})[Cr^{III}(CN)_6]_{2/3}\cdot 4.2H_2O$ and ascribed it to the intra-atomic $d-d$ transition of Co^{2+}. In the fully hole-doped sample [(c) δ=0.61], three optical transitions, that is, 2.4 eV (CT band), 3.1 eV (B band), and 3.7 eV (C band), are observed. Among them, the lowest-lying band (CT band) is ascribed the electron transfer from the Co^{2+} site to the Fe^{3+} site.[10,14,15]

We decomposed the absorption spectra $\alpha(\omega)$ into the four absorption bands,

$$\alpha(\omega) = \sum_{i=A,B,C,CT} \sqrt{\frac{S_i}{2\pi}} \exp\left(-\frac{(\hbar\omega_i - \hbar\omega)^2}{2\Gamma_i^2}\right), \qquad (2)$$

where S_i, $\hbar\omega_i$ and Γ_i are the spectral weight, the resonant energy and the spectral width, respectively. In the fitting procedure, we fixed the values of ω_i and W_i and adjusted magnitude of S_i. The thin solid curves in Fig. 7 are the least-squares-fitted results. In Fig. 8, we plotted the oscillator strength f for these absorption bands against δ. The magnitude of f of the A band linearly decreases with δ, while those of the B, C, and CT bands linearly increase. These δ-dependent behavior indicate that the A band (the B, C, and CT bands) should relate to the Fe^{2+} (Fe^{3+}) species. Especially, the linear increase in S_{CT} with δ is consistent with its

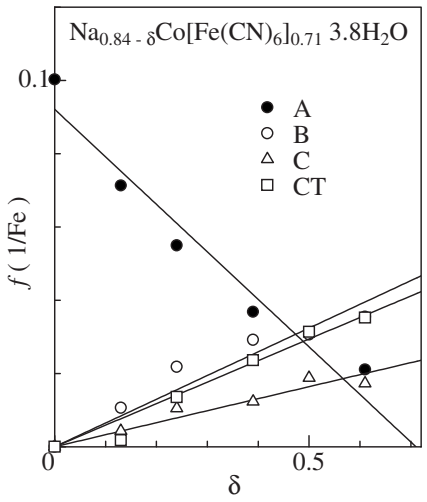

FIG. 8. Oscillator strength f of thin films of $Na_{0.84-\delta}Co[Fe(CN)_6]_{0.71}\cdot 3.8H_2O$ at 300 K. The straight lines are the least-squares-fitted results.

assignment, that is, $Fe^{3+} \rightarrow Co^{2+}$. On the other hand, the higher-lying A band (B and C bands) can be ascribed to the intermolecular transition of $[Fe^{2+}(CN)_6]$ ($[Fe^{3+}(CN)_6]$). We ascribe the B band (the C band) to the electron transfer from CN^- to the unoccupied $t_{2g}(e_g)$ orbital of Fe^{3+} because the energy splitting (=0.58 eV) is reasonable for the crystal-field splitting. In Table I, we listed the parameters of the optical transitions together with the assignment. We note that the magnitude of f(=0.06/Fe) for the CT transition is comparable to that (=0.03/Mn) for the J-gap transition (electron transfer between the neighboring Mn sites) of $La_{0.6}Sr_{0.4}MnO_3$.[25]

IV. DISCUSSION

In this section, we will discuss the δ dependence of the CT transition. Before the discussion, let us summarize the important items observed in the present experiment. First of all, we found that the correlation between T_{CT} and δ is quite weak [see Fig. 5(c)]. This suggests that T_{CT} is mainly governed by the magnitude of the ligand field around the Co site. Second, the ratio of the charge-transferred Co site at the CT transition is δ, as confirmed by the δ dependence of $\mu_{\mathrm{eff}}^{\mathrm{LT}}/\mu_{\mathrm{eff}}^{\mathrm{HT}}$ [see Fig. 5(b)]. Third, we found that the CT transition accompanies the significant reduction in a even at δ=0.13 [see Fig. 5(a)]. This observation strongly suggests that the CT transition is cooperative and uniform, even when a small part of the Co site is charge-transferred. Here, we emphasize that significant reduction of the Co-Fe bond distance is indispensable to stabilize the charge-transferred state, that is, Fe^{2+}-Co^{3+}. Actually, the bond distance decreases from 5.17 to 5.02 Å at the CT transition in the fully hole-doped sample (δ=0.61). Such a bond compression should be ascribed to the concomitant spin state transition of Co^{3+} into the low-spin state (t_{2g}^6). In this sense, the strong coupling between the charge, spin, and lattice degrees of freedom is the key of the CT transition.

TABLE I. Resonance energy $\hbar\omega$ and oscillator strength f of the optical transitions of $Na_{0.84-\delta}Co[Fe(CN)_6]_{0.71}\cdot 3.8H_2O$.

Transition	$\hbar\omega$ (eV)	f	Assignment
A	3.26	0.10/Fe^{2+}	$CN^- \rightarrow Fe^{2+}$ or $Fe^{2+} \rightarrow CN^-$
B	3.14	0.07/Fe^{3+}	$CN^- \rightarrow Fe^{3+}t_{2g}$
C	3.72	0.03/Fe^{3+}	$CN^- \rightarrow Fe^{3+}e_g$
CT	2.41	0.06/Fe^{3+}	$Co^{2+} \rightarrow Fe^{3+}$
D	1.99	0.002/Co	$d-d$ within Co^{2+}
E	2.18	0.003/Co	$d-d$ within Co^{2+}

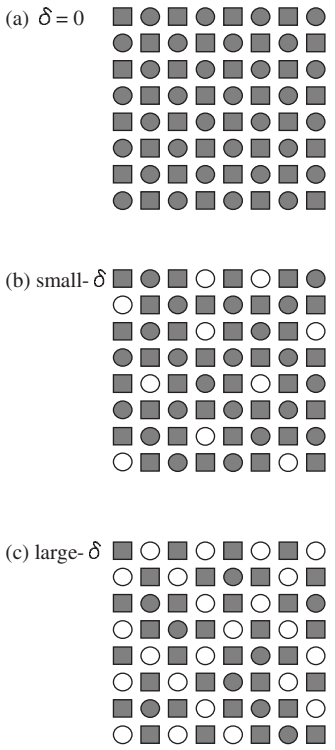

FIG. 9. Schematic illustrations of hole-doped Co^{2+}-Fe^{2+} system: (a) δ=0, (b) small δ, and (c) large δ. Circles and squares represent the Fe and Co site, respectively. White color indicates the hole site (Fe^{3+}).

In Fig. 9, we show schematic illustrations of the hole-doped Co^{2+}-Fe^{2+} system. In larger-δ region [Fig. 9(c)], most of the Fe sites have holes and can transfer an electron to the neighboring Co site. The charge-transfer process accompanies the significant Co-Fe bond compression. The bond compressions should take place cooperatively in order to minimize the distortion energy of the lattice system. As a result, a in the LT phase becomes much shorter than that in the HT phase, causing a high potential barrier between the two phases. Then, the nature of the CT transition in large-δ region is of first-order, as observed in Fig. 5(c).

In small-δ region [Fig. 9(b)], however, only a small part of the Fe site has hole. Nevertheless, the uniform CT transition suggests that the local lattice distortions induced by the charge transfer are weakly connected all over the system in a percolation manner. In such a situation, the lattice-constant change (Δa) at the CT transition should be suppressed as

compared with that in large-δ region. The suppressed Δa causes the second-order nature of the phase transition.

V. SUMMARY

We have derived the electronic phase diagram as a function of the hole concentration δ for thin films of $Na_{0.84-\delta}Co[Fe(CN)_6]_{0.71}\cdot 3.8H_2O$ $(0.0 \leq \delta \leq 0.61)$. We observed the cooperative CT transition in the wide concentration range of $0.13 \leq \delta \leq 0.61$. The nature of the CT transition, however, changes from second-order type in the small-δ region to the first-order type in the large-δ region. The δ dependence of the CT transition was discussed in terms of the coupling between the charge, spin and lattice degrees of freedom. Here, we emphasize that only a small part of the charge transfer can trigger the cooperative phase transition in the present Co-Fe cyanide system. This implies that even the partial charge-transfer induced by photoexcitation may cause a cooperative phase transition. Investigation on this trend is now in progress.

ACKNOWLEDGMENTS

This work was supported by a Grant-In-Aid for Scientific Research from the Ministry of Education, Culture, Sports and Science, Japan and from the Support Center for Advanced Telecommunication (SCAT) Foundation.

*Author to whom correspondence should be addressed; moritomo@sakura.ac.jp

[1] For example, see Y. Tokura and N. Nagaosa, Science **288**, 462 (2000).
[2] P. W. Anderson and H. Hasegawa, Phys. Rev. **100**, 675 (1955).
[3] R. Kajimoto, H. Yoshizawa, H. Kawano, H. Kuwahara, Y. Tokura, K. Ohoyama, and M. Ohashi, Phys. Rev. B **60**, 9506 (1999).
[4] R. Maezono, S. Ishihara, and N. Nagaosa, Phys. Rev. B **58**, 11583 (1998).
[5] R. Maezono and N. Nagaosa, Phys. Rev. B **61**, 1825 (2000).
[6] J. vandenBrink and D. Khomskii, Phys. Rev. Lett. **82**, 1016 (1999).
[7] H. J. Buser, D. Schwarzenbach, W. Petter, and A. Ludi, Inorg. Chem. **16**, 2704 (1977).
[8] O. Sato, Y. Einaga, T. Iyoda, A. Fujishima, and K. Hashimoto, J. Phys. Chem. B **101**, 3903 (1999).
[9] In the electrochemical point of view, the "holes" are introduced on the Fe site by the oxidization of Fe^{II} in the present system. In this paper, however, we are interested in the physical properties of the oxidized "hole-doped" product, not in the actual electrochemical process. We use the expression, "hole doping" by the removal of Na, in the following reasons. First, we regard the cyano-bridged transition-metal system as a valence-tunable *d*-electron system, similar to the perovskite oxide system, $R^{3+}_{1-x}A^{2+}_{x}MO_3$ (*R*, *A*, and *M* are a rare-earth metal, an alkaline-earth metal, and a transition metal, respectively.) In the oxide system, the hole doping is performed by the chemical substitution of A^{2+} for R^{3+}. Similarly, the hole doping in the present system is performed by the substitution of $\square^0$ (vacancy) for Na^+. Second, the oxidized transition metal depends on the chemical composition even in the Co-Fe cyanide. Actually, we found that the "holes" are introduced on the Co site by the oxidization of Co^{II} in the vacancy-reduced Co-Fe cyanide films (to be published). In this sense, the "holes" are introduced on the cyano-bridged network or the *d*-electrons system.
[10] N. Shimamoto, S. Ohkoshi, O. Sato, and K. Hashimoto, Inorg. Chem. **41**, 678 (2002).
[11] O. Sato, T. Iyoda, A. Fujishima, and K. Hashimoto, Science **272**, 704 (1996).
[12] O. Sato, Y. Einaga, A. Fujishima, and K. Hashimoto, Inorg. Chem. **38**, 4405 (1999).
[13] M. Hanawa, Y. Moritomo, A. Kuriki, J. Tateishi, K. Kato, M. Takata, and M. Sakata, J. Phys. Soc. Jpn. **72**, 987 (2003).
[14] T. Yamauchi, A. Nakamura, Y. Moritomo, T. Hozumi, K. Hashimoto, and S. Ohkoshi, Phys. Rev. B **72**, 214425 (2005).
[15] Y. Moritomo, F. Nakada, H. Kamioka, T. Hozumi, and S. Ohkoshi, Phys. Rev. B **75**, 214110 (2007).
[16] H. Kamioka, Y. Moritomo, W. Kosaka and S. Ohkoshi, Phys. Rev. B **77** 180301(R) (2008).
[17] E. Nishibori, M. Takata, K. Kato, M. Sakata, Y. Kubota, S. Aoyagi, Y. Kuroiwa, M. Yamakawa, and N. Ikeda, Nucl. Instrum. Methods Phys. Res. A **467-468**, 1045 (2001).
[18] E. Reguera, J. F. Bertran, C. Diaz, and J. Blanco, Hyperfine Interact. **53**, 391 (1990).
[19] K. Kato, Y. Moritomo, H. Tanaka, H. Tokoro, S. Ohkoshi, and M. Takata, J. Phys. Soc. Jpn. **76**, 123602 (2007).
[20] Strictly speaking, the melting temperature T_m is not the critical temperature for the phase transition. T_m is a characteristic temperature where the relaxation time from the metastable phase to the stable phase becomes comparable to the experimental time scale (order of minute).
[21] T. Kawamoto, Y. Asai, and S. Abe, Phys. Rev. Lett. **86**, 348 (2001).
[22] J. W. Essam, in *Phase Transition and Critical Phenomena*, edited by C. Domb and M. S. Green (Academic, London, 1972), Vol. 2, p. 197.
[23] T. Kawamoto, Y. Asai, and S. Abe, Phys. Rev. B **60**, 12990 (1999).
[24] S. Ohkoshi, K. Arai, Y. Sato, and K. Hashimoto, Nat. Mater. **3**, 857 (2004).
[25] Y. Moritomo, A. Machida, K. Matsuda, M. Ichida, and A. Nakamura, Phys. Rev. B **56**, 5088 (1997).